MMD
JOURNAL / MINING.IN.UA

Numerical simulation of mechanical behavior of rock samples under uniaxial and triaxial compression tests

Wael R. Abdellah[1]*✉ iD, Salah A. Bader[2]✉, Jong-Gwan Kim[3,4]*✉, Mahrous A.M. Ali[5]✉ iD

[1] Department of Mining and Metallurgical Engineering, Faculty of Engineering, University of Assiut, Assiut, Egypt
[2] Mining and Petroleum Engineering Department, Faculty of Engineering- Cairo, Al-Azhar University, Cairo, Egypt
[3] Chonnam National University, Gwangju, South Korea
[4] CHAORUM Planning & Development Co., Ltd., Gwangju, South Korea
[5] Mining and Petroleum Engineering Department, Faculty of Engineering-Qena, Al-Azhar University, Qena, Egypt
*Corresponding author: e-mail waelabdellah@aun.edu.eg, kimjg@chonnam.ac.kr

Abstract

Purpose. The research aims to investigate how the load influences the ultimate compressive strength of rocks at failure. It uses both a uniaxial compression test, which involves incremental displacements, and a triaxial compression test, which applies varying confining stresses while maintaining a constant axial compression stress and incrementally increasing the displacement.

Methods. To conduct the investigation, the researchers used RS^{2D}, a rock-soil software, to examine the impact of different incremental displacements and confining stresses on the strength properties of various rock samples. The numerical analysis includes Fayum argillaceous sand, Sinai coal, Aswan granite, Assiut limestone, and Red-Sea phosphate.

Findings. The research findings indicate that the ultimate compressive strength of rocks at failure is achieved with minor incremental displacements. Conversely, an increase in the confining stress leads to higher ultimate tensile strength, deviatoric stresses, and volumetric strain. However, the stress factor decreases in relation to the axial strain percentage.

Originality. The simulator adopts Mohr-Coulomb failure criterion, presents and discusses the results in terms of stress-strain (σ-ε) curves, stress ratio (σ_1/σ_3), deviatoric stresses ($\sigma_1-\sigma_3$) and volumetric strain with respect to the percentage of axial strain.

Practical implications. Using numerical modeling analysis, it becomes possible to reproduce the rock failure mechanisms observed in uniaxial and triaxial compression tests. This methodology has the potential to reduce the need for extensive experimental testing when assessing the tensile strength of rocks under different loads. As a result, both time and costs can be minimized.

Keywords: uniaxial and triaxial compression tests, numerical modeling, displacement/strain rate, confining stresses, stress-strain curves, deviatoric stress

1. Introduction

One of the most well-known tools for determining the mechanical properties of intact rocks is experimental tes-ting [1]-[3]. These tests shed light on the rock failure mechanism under mechanical loading [4], [5]. Yet, the formation of microcracks, as well as their propagation and coalescence in rock samples, is not completely understood [6], [7]. Large-scale experimental investigation of rock behaviour is difficult. Hence, numerical modelling approaches can be effectively used as an alternate tool for examining rock attributes (strength, deformability, etc.) under varied loading conditions [8], [9]. For decades, numerical simulation methods have been considered the state of the art in rock mechanics. With the expansion of possibilities and, as a result, the complication of the existing constitutive laws, the determination of accurate input parameters has become increasingly important. Rock is a crucial facet of the rock mass, and its influence on the mechanical properties of the entire mass is primarily dictated by its own mechanical properties. Stress and strain factors, as well as failure features such as strength, deformation and resilience are examples of

such attributes. The strength and deformation attributes of rocks are the most important. Rock strength (e.g., compressive, tensile, and/or shear strength) determines the resistance of rock to deformation under specific applied loads/stresses, whereas rock deformation is a change in size and shape, which in turn determines the elastic brittle (e.g., coal), elastoplastic, flowing, creeping, and/or relaxation behaviour of rock [10]-[12].

According to Lockner and Hoek [13], [14] the strength and deformation moduli of rocks are required in practically all mining, earth sciences, and civil engineering analyses (e.g., design of rock slope, design of rock support systems, underground excavations, tunneling, and foundations). Rock is an anisotropic heterogeneous material with multiple pre-existing fractures ranging in size from the micro (e.g., microscopic cracks) to the macroscale (e.g., faults). As a rock is loaded or compressed, it exhibits several rock behaviors (phenomena), such as elastic deformation (e.g., pre-loading region and beginning of loading), stress propagation and redistribution, fracture extension and coalescence, and post-failure behaviour (e.g., strain-hardening or softening and yielding) [15], [16].

When a rock is uniaxially crushed, it exhibits several rock failure modes and processes (spalling, splitting, and oblique) [17]. The mechanisms of rock spalling and splitting suggest tensile failure, whereas the oblique mode implies shear failure. On the microscale, interactions between minor fissures can cause shear or tensile failure modes [18]. Confining (lateral) stress inhibits the development of tensile cracks under biaxial loading, resulting in the expansion of dense pre-existing cracks. As a result, the brittle shear failure mode causes macrofractures in the rock [19], [20]. The unconfined (UCS) and triaxial compressive strength are the most important criteria in assessing rock material behaviour. As a result, understanding fractured rock failure mechanisms requires knowledge of the UCS and triaxial. An effective approach for estimating the UCS and analyzing the behaviour of rock materials under unconfined and triaxial compression is necessary in the majority of rock mechanics research domains. The experiments were replicated using the finite element method (FEM). Because of its potential for dealing with substantial deformation concerns in rocks, this approach is employed in this research. The finite-element analysis entails a continuum mechanics method and excludes the various other approaches that are now available. To produce realistic simulation results, a thorough understanding of the stress-strain curve for a variety of loading conditions is essential. As a result, this research gives a way for using numerical modelling approaches to identify the behaviour of rock mass under uniaxial and triaxial loads up to failure. Hence, mine planners will be able to predict when and where a rock mass will require support during the life of underground structures.

The purpose of this research is to replicate the behaviour (failure process and deformation) of anisotropic heterogeneous rock samples using the finite-element method of analysis. The focus of this research is to numerically estimate the ultimate rock strength at failure in uniaxial and triaxial compression tests at different loading rates (e.g., incremental displacements and confining stresses). The experimentally intact rock values are converted to rock mass parameters compliant with the generalized Hoek-Brown criterion using built-in tables and charts integrated in the RocLab application. Charts and tables show the rock geological strength index as well as the disturbance factor based on rock type and geological circumstances. Because the Mohr-Coulomb criterion is the most widely employed function for evaluating failure. As a result, RocLab includes a tool that allows users to calculate rock mass values using the equivalent Mohr-Coulomb failure envelope. The obtained rock mass is then employed in the Rock-soil (RS^{2D}) finite element code [21], which applies the Mohr-Coulomb elastoplastic failure criterion, to calculate cohesion, friction angle, tensile and compressive strengths, and elastic modulus. It should be noted that the effect of anisotropy (such as sample size, loading direction, discontinuities, stratification, and foliation) falls outside the scope of this study.

The remainder of the manuscript is organized as follows: Part 2: Materials and Methods Part 3: Results and Discussions and Section 4 will provide the conclusions.

2. Materials and methods

Rock samples were gathered in Egypt from various locations. Limestone was taken from the Assiut Cement Company Quarry, granite from Aswan, phosphate from Safaga city in the Red-Sea governorate, coal from the El-Maghara coal mine in the Sinai desert about 250 km north-east of Cairo, and argillaceous sand from the Qasr El Sagha Delta in Fayum, Egypt. Each type of rock was cut into blocks around 20×15×10 cm in size using a diamond saw. The rocks were then cored using a core diamond machine at Assiut University's Mining Department's Rock Mechanics Lab. Density, porosity, compressive strength, tensile strength, and coefficient of internal friction (μ) were found as the most essential physical and mechanical parameters of the studied rocks.

The intact rock values are then converted to rock mass properties using RocLab software. RocLab is a Rocscience Inc. product. It is employed for calculating rock mass strength parameters based on the generalized Hoek-Brown failure criterion [22]. Such criterion is implemented in RocLab in a straightforward and user-friendly manner, allowing users to efficiently obtain reliable estimates of rock mass properties and visualize the effects of changing rock mass parameters on failure envelopes. RocLab calculates equivalent Mohr-Coulomb parameters from the Hoek-Brown failure envelope. It is applicable to all types of rocks, including the applicability to very weak rock. Typically, determining the properties of rock mass is done by RocLab to provide input data for numerical analysis programs [23], [24]. The following are the steps for obtaining rock mass properties using RocLab:

1. Generalized Hoek-Brown strength parameters of a rock mass (*mb*, *s* and *a*) are first calculated based on the intact rock properties, intact rock parameter (*mi*), geological strength index (GSI) and disturbance factor (*D*). The *mi*, GSI, and *D* parameters are obtained from RocLab's built-in charts and tables based on rock type and geological conditions. These charts and tables can be accessed by clicking the "Pick" button next to each of the input parameter edit boxes in the sidebar. When the user clicks the "Pick" button, a table or chart appears, allowing the user to determine an appropriate value for the desired parameter. Another feature of RocLab is the ability to enter triaxial lab test data (σ_1 and σ_2 data pairs) to calculate the intact rock parameter, *mi*.

2. Failure envelopes of rock masses will be plotted as:
– principal stress space (σ_1 *vs*, σ_1);
– shear – normal stress space (τ, *vs*, σ_n);
– equivalent Mohr-Coulomb failure envelope.

3. Because most rock engineering software is still written in terms of the Mohr-Coulomb failure criterion. Therefore, RocLab includes a feature that calculates equivalent Mohr-Coulomb rock mass parameters (e.g., cohesion, friction angle, deformation modulus, tensile and uniaxial compressive strengths) from the Hoek-Brown failure criterion.

4. The RocLab-derived rock mass properties are then used as input parameters in Rock-Soil (RS^{2D}) finite element code.

In this analysis, two-dimensional elastoplastic finite-element models were created using the RS^{2D} program to simulate the mechanical behavior of rock samples (ultimate strength and moduli of elongation at failure) subjected to uniaxial and triaxial compression at multiple incremental displacements and various confining stresses. Rock-Soil (RS2) is a 2D Rocscience finite element code which is used for stress/deformation analysis, surface and underground excavation stability, support design, dams, and soil slope assessment. RS2 includes all of the tools required to conduct a true dynamic study of geotechnical structures subjected to earthquakes or other dynamically applied loads. Rayleigh and hysteretic damping, excess pore pressure creation, sophisticated dynamic constitutive models that capture liquefaction, natural frequencies analysis, and dynamic data analysis are among the techniques used. RS2 uses the extended finite

element method (XFEM) to represent joint boundaries and networks that aren't constrained by the finite element mesh. Narrow or intricate joint patterns can be simulated much faster than previously without the requirement for a fine mesh. Liquefaction, mining, tunnelling, and foundations are all areas where this program can be used. The modeling setup for a rock sample loaded uniaxially and triaxially is presented in the following sub-sections.

2.1. Uniaxial compression test

This test was conducted to evaluate rock strength properties such as unconfined compressive strength and moduli of elasticity (as it directly relates to the stress-strain characteristics of the tested rock). The rock samples were prepared (polish, shape, length, and diameter) axccording to the standards of the American Society for Testing and Materials (ASTM D3148 and D2938) and the International Society for Rock Mechanics (ISRM). Then, the test was conducted by applying a uniaxially increasing load while maintaining a constant stress rate (between 0.5 to 1 MPa/s.). During the compression test, both axial and radial (diametrical) strains can be measured with high accuracy (5×10^{-6}). It is recommended that loading/unloading cycles be implemented to obtain the most accurate values of rock strength properties [25]. In this investigation, the rock specimen had a diameter of 50 mm and a height-to-diameter ratio of 2.0, as shown in Figure 1 (left). Owing to the advantage of symmetry by modeling half of the domain, as shown in Figure 1 (right), symmetry was only applied if the loading and geometry were symmetrical.
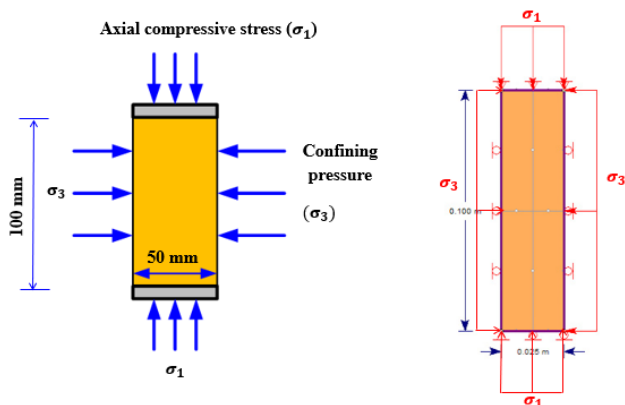
Figure 1. Dimensions, boundary conditions, and symmetry of rock sample under the uniaxial compression test

2.2. Triaxial compression test

The objective of this test was to examine the influence of different confining pressures (σ_3) on the mechanical behavior of rock samples (ultimate strength at failure). The dimensions of the rock specimens were kept identical to those subjected to the uniaxial compression test (width × height: 50×100 mm). The rock samples subjected to triaxial compression tests were prepared based on the ASTM and ISRM standards (ASTM D2664 and D5407). The rock sample was placed into a triaxial chamber contained in a rubber sealing membrane and subjected to an isotropic lateral pressure, and an axial load was subsequently applied [9], [26]. Figure 2 illustrates the modeling setup for the rock specimens under the triaxial compression test. Table 1 lists the mechanical properties of the rock samples used in the analysis. The different incremental displacements and axial and confining stresses applied in this study are listed in Table 2.
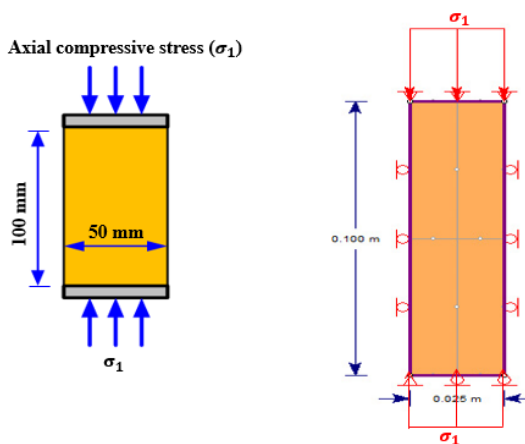
Figure 2. Dimensions, boundary conditions, and symmetry of rock sample under the triaxial compression test

3. Results

This section is divided into two parts: the first part presents the effect of different incremental displacements on the ultimate rock strength at failure subjected to a uniaxial compression load, and the second part introduces the influence of different confining (lateral) stresses on the rock strength properties at failure under the triaxial compression load. As mentioned previously, plane strain models were built using the RS^{2D} program [21].

Table 1. Experimentally obtained physical and mechanical properties of studied rocks

Parameter	Unit	Value				
		Fayum argillaceous sand	Sinai coal	Red-Sea phosphate	Assiut limestone	Aswan granite
Mass density	kg/m^3	1700	1320	2100	2220	2700
Young's modulus	GPa	6.70	1.30	6.00	14.40	59.00
Poisson's ratio		0.31	0.28	0.25	0.28	0.26
Tensile strength	MPa	2.60	1.15	3.10	7.50	11.60
Cohesion	MPa	6.30	1.90	11.20	17.50	14.80
Internal friction angle	Degrees	35.0	30.0	30.0	33.5	63.0

Table 2. Simulated parameters of the numerical modeling process for each compression test

Rock	Uniaxial compression test		Triaxial compression test	
	Incremental displacements, m	Axial stress, KPa	Confining stress, KPa	Displacement rate, m
Fayum argillaceous sand	0.0005, 0.00075, 0.005	200	100, 150, 200	0.0005
Sinai coal	0.0005, 0.001, 0.005	750	100, 200, 300, 500, 750	0.0005
Red-Sea phosphate	0.001, 0.003, 0.005, 0.008	250	100, 200, 300	0.001
Assiut limestone	0.0005, 0.00075, 0.001, 0.005	500	100, 250, 500	0.0005
Aswan granite	0.0005, 0.00075, 0.001	12000	500, 1000, 2000, 4000, 6000	0.0005

And half of the model domain was simulated (owing to the advantage of symmetry). The simulated model dimensions were 25×100 mm (width × height) and were divided into 10000 elements (50×200).

3.1. Effect of incremental displacements (uniaxial compression test)

In this section, the results of the mechanical behavior of five rock samples (Fayum argillaceous sand, Sinai coal, Red-Sea phosphate, Assiut limestone, and Aswan granite) under uniaxial loading and different incremental displacements are presented and discussed. The axial strain is estimated from the vertical displacement (axial strain is defined as the ratio of change in length to the initial or original length, $\varepsilon_y = \dfrac{\Delta y}{Y}$), as shown in Figure 3.
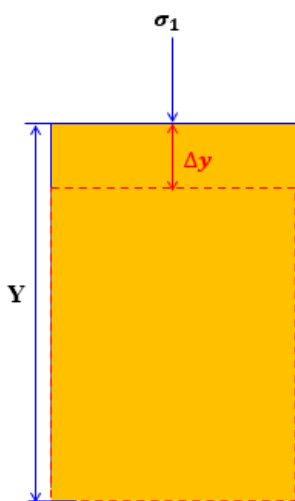
Figure 3. Estimating the axial strain from the vertical displacement ($\varepsilon_y = \dfrac{\Delta y}{Y}$)

The stress-strain curves for different rocks at variable incremental displacements (strain rates) are shown in Figure 4. The final compressive strength of the examined Fayum argillaceous sand specimens varies with incremental displacements. Alternatively, when incremental displacement increases, the compressive strength of the rock sample decreases, and vice versa. At incremental displacements of 0.005 m (with an axial strain of 0.30%), 0.00075 m (with an axial strain of 0.315%), and 0.0005 m (with an axial strain of 0.32%), respectively, the ultimate compressive strengths of the Fayum argillaceous sand samples are 24.32, 25.32 and 25.71 MPa. The ultimate compressive strength of the Sinai coal rock at different incremental displacements (0.0005, 0.001, and 0.005 m) indicates that when uniaxially compressed at a large incremental displacement, the Sinai coal fails early (at a low compressive strength). For example, the values of the ultimate compressive strength of the tested Sinai coal samples at failure are 6.38, 6.28 and 6.0 MPa at incremental displacements of 0.0005 m (with an axial strain of 0.43%), 0.001 m (with an axial strain of 0.42%), and 0.005 m (with an axial strain of 0.40%), respectively.

When uniaxially loaded at a high incremental displacement, the stress-strain curves for Red-Sea phosphate rock at various incremental displacements clearly reveal that the Red-Sea phosphate specimen fails at a low ultimate compres-

sive strength. The ultimate compressive strengths of Red-Sea phosphate rock at failure are 36.33 MPa (at an incremental displacement of 0.001 m and an axial strain of 0.56%), 35.32 MPa (at an incremental displacement of 0.003 m and an axial strain of 0.54%), 32.72 MPa (at an incremental displacement of 0.005 m and an axial strain of 0.50%), and 31.42 MPa (with an incremental displacement of 0.008 m and an axial strain of 0.48%). When the ultimate compressive strength of Assiut limestone is compared to the axial strain percent, it can be shown that as the incremental displacement grows, the final compressive strength of Assiut limestone falls. Compressive strengths of Assiut limestone rock are 63.61 MPa (with incremental displacements of 0.0005 m and 0.00075 m and an axial strain of 0.39%), 62.48 MPa (with an incremental displacement of 0.001 m and an axial strain of 0.38%), and 53.45 MPa (with an incremental displacement of 0.001 m and an axial strain of 0.38%).

The axial compressive strengths of Aswan granite rock at failure at multiple axial strain percentages indicate that the magnitudes of ultimate compressive strength of Aswan granite at failure are 126.45 MPa (with an incremental displacement of 0.0005 m and an axial strain of 0.16%), 120.04 MPa (with an incremental displacement of 0.00075 m and an axial strain of 0.15%), and 126.45 MPa (with an incremental displacement of 0.001 m and an axial strain of 0.16%). On the basis of these findings, it may be stated that rock's ultimate compressive strength varies with loading rate (incremental displacement/strain rate). For example, the compressive strength of Fayum argillaceous sand at failure varies between 24.32 and 25.32 MPa, while the compressive strength of Sinai coal varies between 6.0 and 6.38 MPa, Red-Sea phosphate's compressive strength varies between 31.42 and 36.33 MPa, Assiut limestone's compressive strength varies between 53.45 and 63.61 MPa, and Aswan granite's compressive strength varies between 120.04 and 126.45 MPa.

3.2. Influence of confining pressure (triaxial compression test)

Many authors have stated that the confining pressure (σ_3) is proportionally related to the axial compressive stress at failure (σ_1) and that rock will exhibit a gradual transition from brittle to ductile behaviors [27], [28]. To investigate the impact of confining pressure on the ultimate compressive strength of rock at failure, five rock specimens were subjected to diffe-rent confining pressures and single-value axial stress and displacement rates (Table 2). In the following section, the results are presented and discussed in terms of the stress-strain ($\sigma - \varepsilon$) curves, stress ratios (σ_1 / σ_3), deviatoric stresses ($\sigma_1 - \sigma_3$), and volumetric strain against the axial strains.

3.2.1. Stress-strain ($\sigma - \varepsilon$)

Figure 5 depicts the axial compressive strength of rock specimens at failure against the axial strain percent. It can be observed that the ultimate compressive strength slightly increases as the confining stress increases. For example, the values of ultimate compressive strength of Fayum argillaceous sand are 25.75 MPa (with a confining stress of 200 KPa and an axial strain of 0.32%), 25.74 MPa (with a confining stress of 150 KPa and an axial strain of 0.32%), and 25.73 MPa (with a confining stress of 100 KPa and an axial strain of 0.32%).
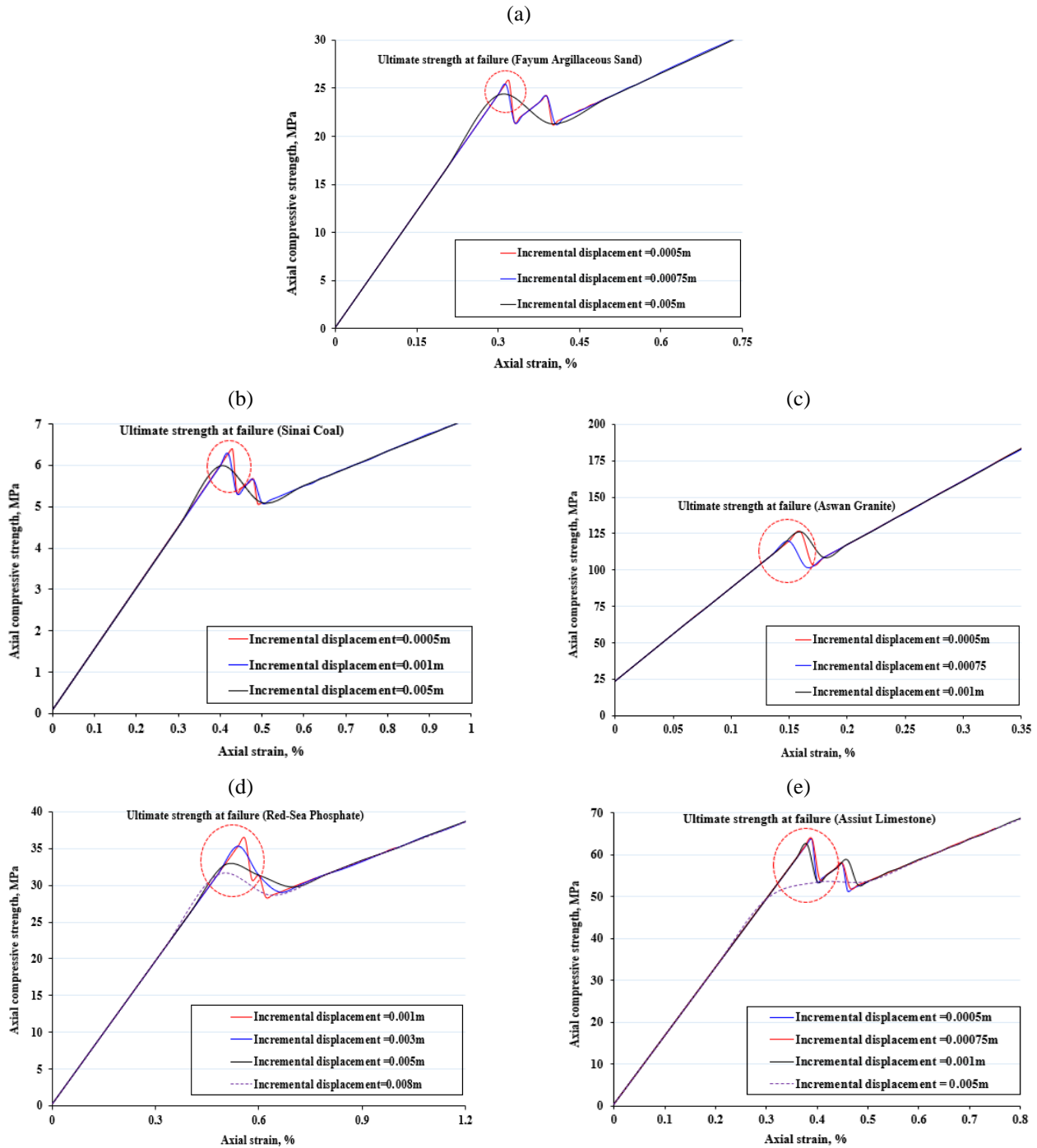
Figure 4. Stress-strain curves for different rock specimens at various incremental displacements: (a) Fayum argillaceous sand; (b) Sinai coal; (c) Aswan granite; (d) Red-Sea phosphate; (e) Assiut limestone

The ultimate compressive strength of the Sinai coal at failure increases as the confining stress increases. For example, the magnitudes of the maximum compressive strength of Sinai coal are 7.69, 7.13, 6.91, 6.65 and 6.55 MPa at confining stresses of 750, 500, 300, 200 and 100 KPa, respectively. The ultimate compressive strength of Red-Sea phosphate at failure increases slightly as the confining stress increases. For example, the values of the maximum compressive strength of Red-Sea phosphate are 35.35, 35.33 and 35.32 MPa at confining stresses of 300, 200 and 100 KPa, respectively. For Assiut limestone, the axial compressive strength shows that the magnitudes of the ultimate compressive strength insignificantly vary from 64.13 to 65.29 MPa at confining stresses of 100 to 500 KPa, respectively. For Aswan granite, it can be seen that the compressive strength

significantly increases as the confining stress increases. For example, the magnitudes of the compressive strength of Aswan granite specimens at failure are 236.30, 203.95, 165.20, 145.83 and 132.93 MPa at confining stresses of 6000, 4000, 2000, 1000 and 500 KPa, respectively.

3.2.2. Deviatoric stress ($\sigma_1 - \sigma_3$)

The deviatoric stress is defined as the difference between the axial and lateral stress ($\sigma_1 - \sigma_3$). It produces shear stress, which may lead to plastic flow if it exceeds the elastic limit of the rock. The deviatoric stress causes no dilation, as the sum of its components is always zero. Figure 6 depicts the deviatoric (differential) stresses at various confining stresses against the axial strain percent for all rock samples.
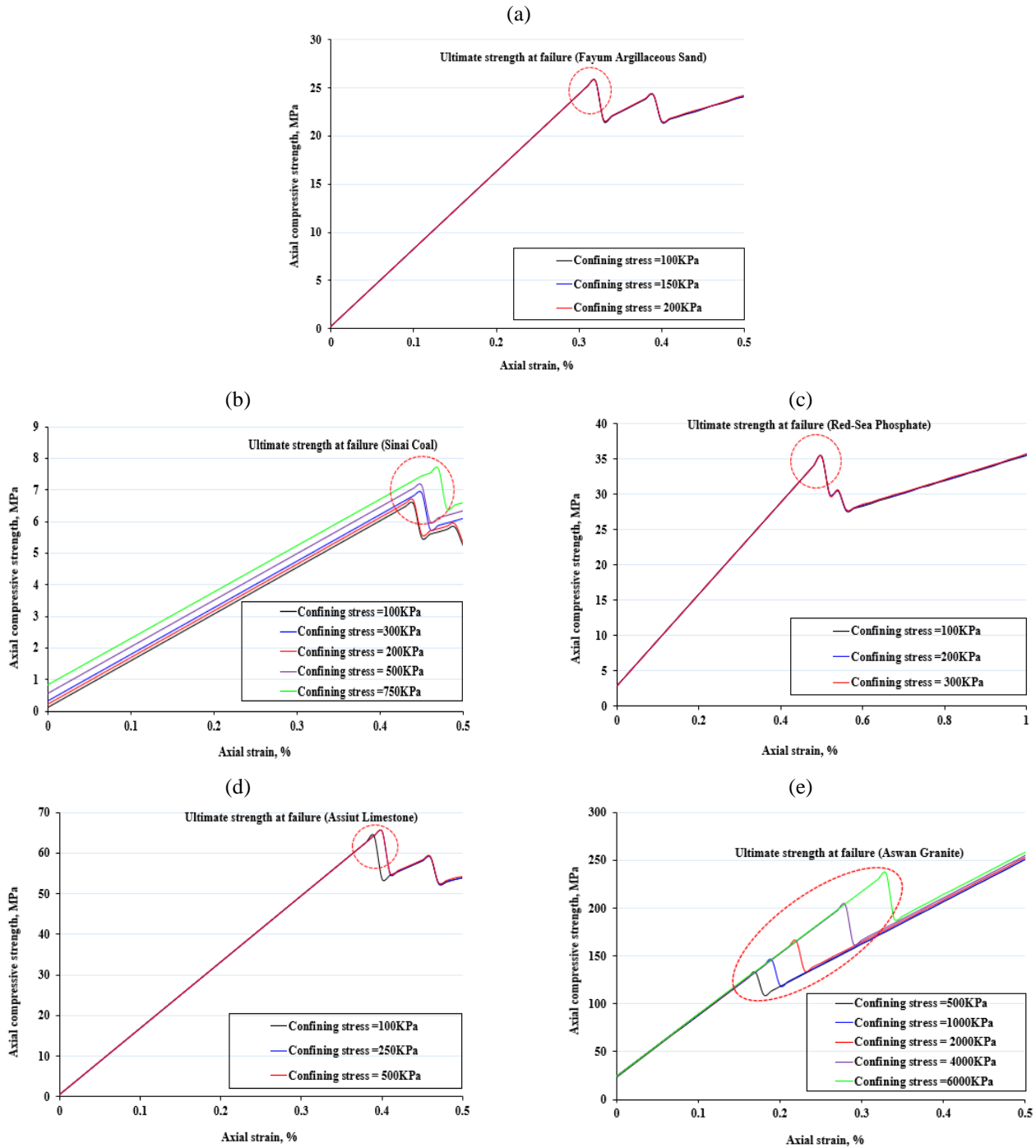
Figure 5. Axial compressive strength of all tested rock samples against the axial strain percent at various confining stresses and constant incremental displacements: (a) Fayum argillaceous sand; (b) Sinai coal; (c) Red-Sea phosphate; (d) Assiut limestone; (e) Aswan granite

For Fayum argillaceous sand, it can be seen that there is no change in the magnitude of the deviatoric stress at different lateral pressures. The maximum deviatoric stress is 14.87 MPa at an axial strain percent of 0.32 and multiple confining stresses. For Sinai coal, Red-Sea phosphate, Assiut limestone and Aswan granite, it can be observed that the deviatoric stress increases as the confining stress increases. Thus, it is evident that the deviatoric stresses significantly increase as the lateral pressure increases.

3.2.3. Stress ratio (σ_1 / σ_3)

Figure 7 illustrates the relationship between the stress ratio and axial strain under various confining stresses. In the case of Fayum Argillaceous sand, an increase in axial strain percentage leads to a decrease in the stress ratio. The value of the stress ratio is not significantly affected by the confining stress. Regarding Sinai coal, an increase in confining stress results in an increase in the stress ratio, but as the axial strain percentage rises, the stress ratio decreases.

A similar trend can be observed for Red-Sea phosphate, where the stress ratio increases with increasing confining stress but decreases with increasing axial strain percentage. When considering Assiut limestone, it is evident that the stress ratio decreases as the axial strain percentage increases. Finally, for Aswan Granite, a clear observation is that the stress ratio decreases significantly with an increase in the axial strain percentage.
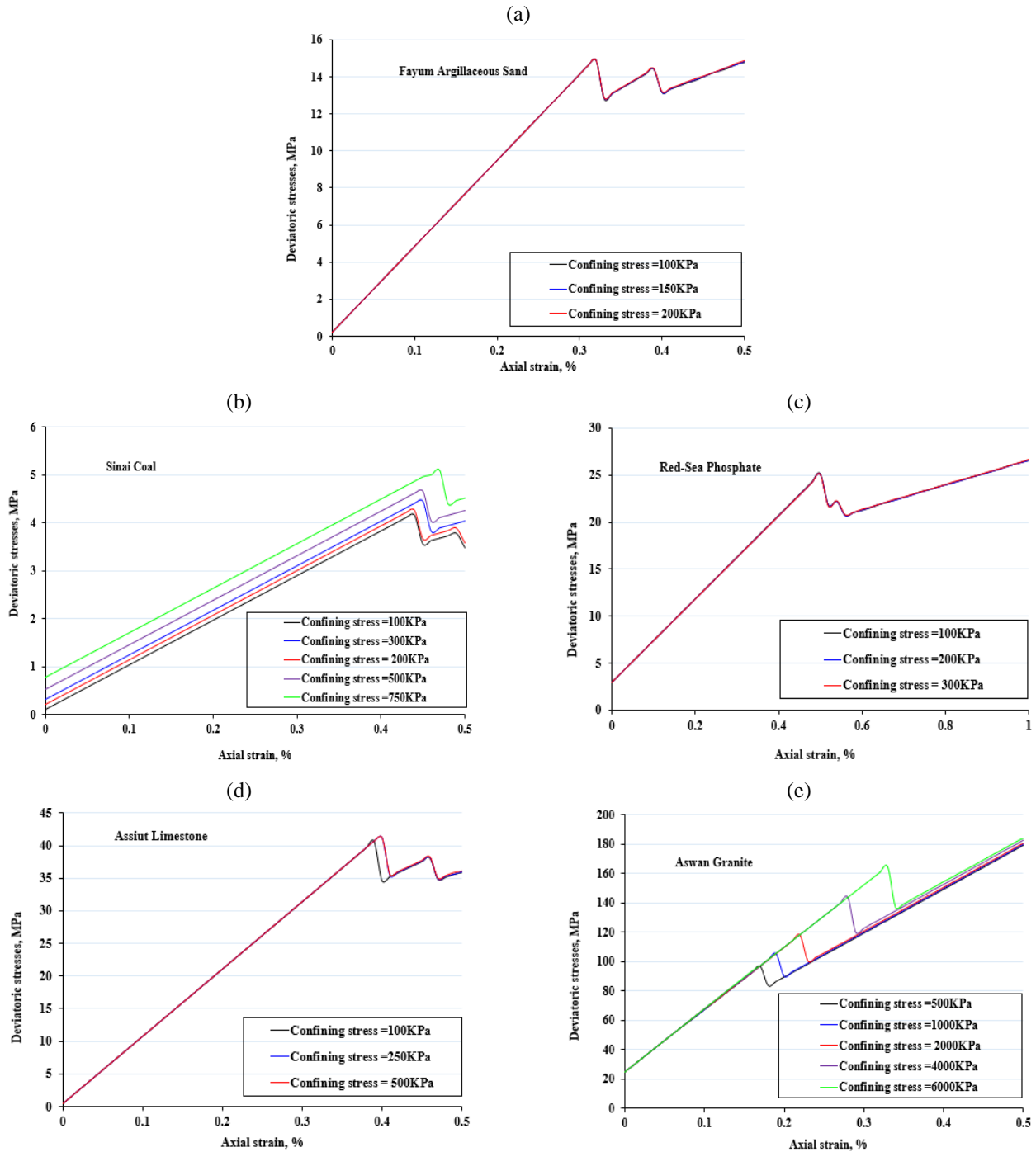
Figure 6. Deviatoric stress versus axial strain percent at various confining pressures for different rock samples: (a) Fayum argillaceous sand; (b) Sinai coal; (c) Red-Sea phosphate; (d) Assiut limestone; (e) Aswan granite

3.2.4. Volumetric strain

The volumetric strain, which characterizes the change in rock volume during compression, determines the stress level at which the instantaneous rate of volumetric change becomes zero. This occurs when the slope of the volumetric strain curve changes its sign. Figure 8 illustrates the relationship between axial and volumetric strains under different confining pressures. In the case of Fayum Argillaceous sand, an increase in axial strain results in an increase in volumetric strain.

Higher confining pressures lead to positive volumetric strains. When examining Sinai coal, it can be observed that the volumetric strain increases with axial strain. The maximum volumetric strain is 0.0047, while the minimum is 0.0044. Regarding Red-Sea phosphate, the volumetric

strain shows insignificant growth with increasing confining stress but increases with axial strain percentage. As for Assiut limestone, it is evident that the volumetric strain increases as the axial strain percentage rises. Finally, for Aswan granite, there is a clear indication that both confining stresses and axial strain contribute to a significant increase in volumetric strain.

4. Discussion

This study utilizes numerical simulations as an alternative to traditional laboratory testing in rock mechanics. It examines the behavior of rocks under uniaxial and triaxial compression and investigates the impact of confining pressure and loading rate on the stress-strain curve and ultimate strength at failure.

(a)

(b)   (c)

(d)   (e)
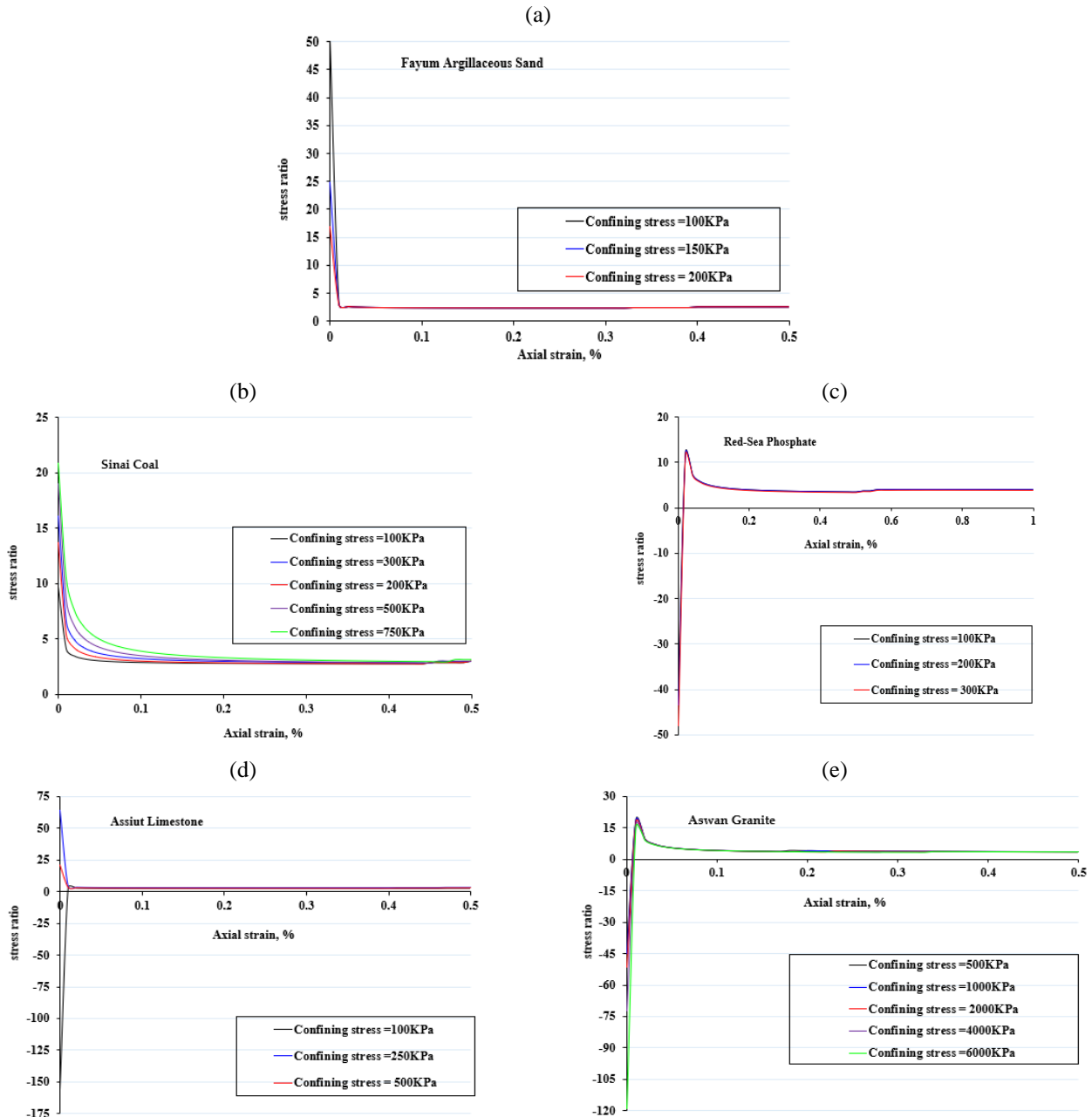
Figure 7. Stress ratio of different rock specimens at various confining pressures with respect to axial strain percent: (a) Fayum argilla-ceous sand; (b) Sinai coal; (c) Red-Sea phosphate; (d) Assiut limestone; (e) Aswan granite

The researchers employ the finite element RS2D (Rock-soil) software to simulate the physical experiment on rocks, providing several advantages over traditional experiments. Numerical simulations serve as a substitute means of investigation in rock mechanics, offering a reliable alternative to physical testing. In the case of uniaxial compression tests, conducted at the lowest loading rate (e.g., incremental displacement of 0.0005 m), the ultimate uniaxial compressive strengths for Fayum argillaceous sand, Sinai coal, Red-Sea phosphate, Assiut limestone, and Aswan granite were determined as 25.71, 6.38, 36.59, 63.61 and 126.45 MPa, respectively (Fig. 9). On the other hand, under triaxial compression tests, it was observed that the ultimate strength of the rocks at failure increased with increasing confining stress (Table 3).

For instance, the ultimate compressive strengths for Fayum argillaceous sand, Sinai coal, Red-Sea phosphate, Assiut limestone, and Aswan granite were found to be 25.75, 7.69, 35.35, 65.29 and 236.30 MPa, respectively.
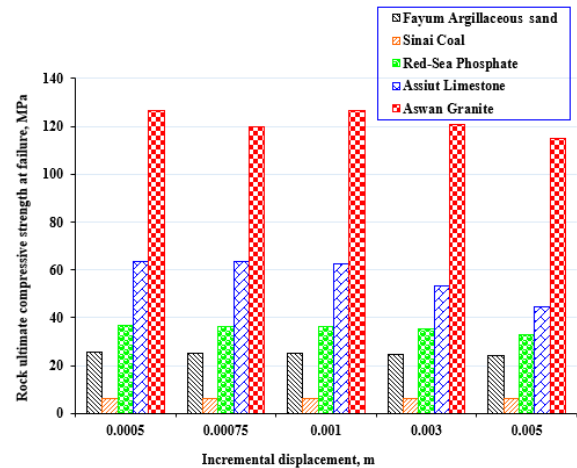
Figure 9. Ultimate compressive strength of simulated rocks at failure against various incremental displacements (under uniaxial compression test)
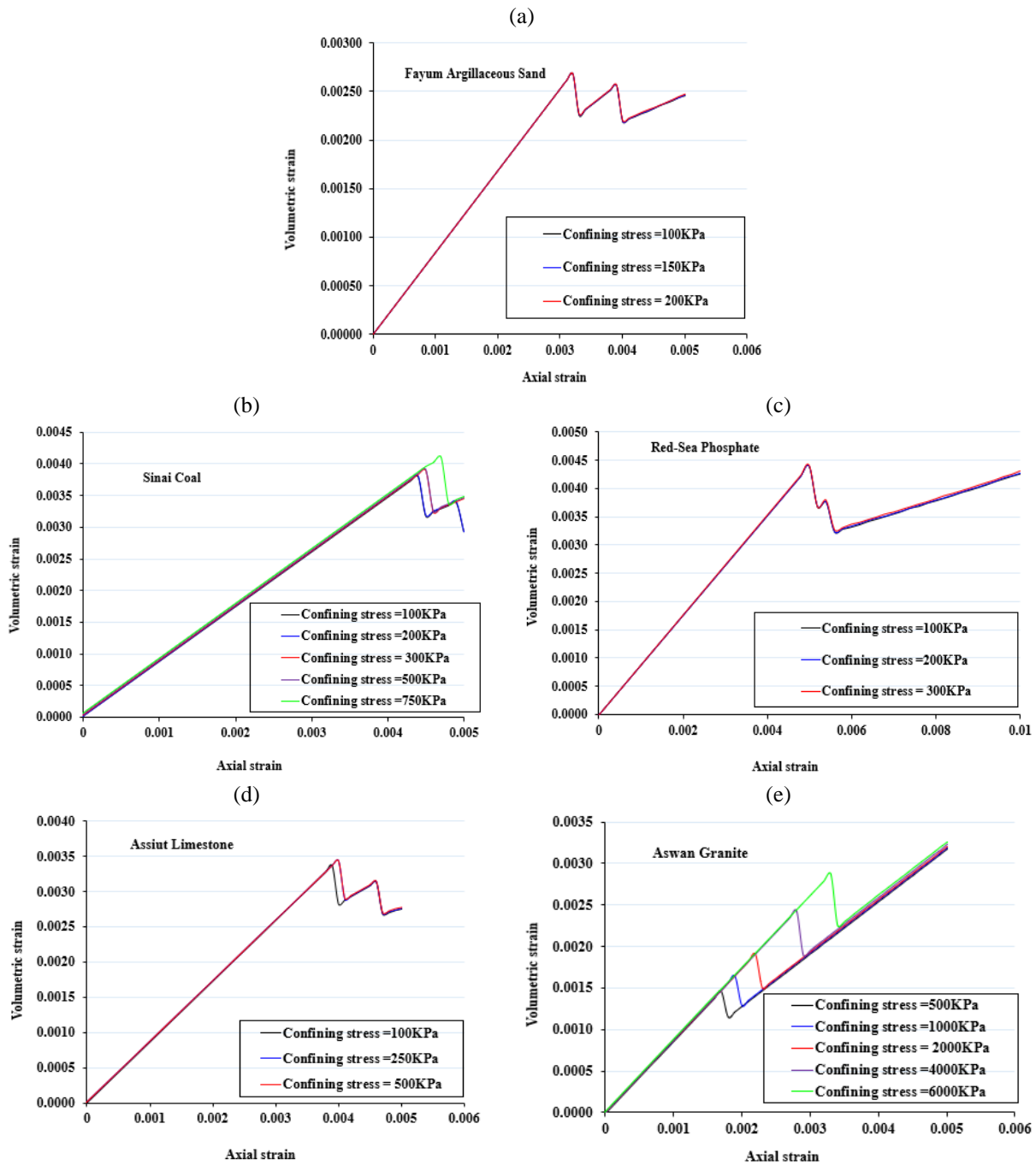
Figure 8. Volumetric strain versus axial strain at different confining pressures for different rock specimens: (a) Fayum argillaceous sand; (b) Sinai coal; (c) Red-Sea phosphate; (d) Assiut limestone; (e) Aswan granite

Table 3. Ultimate compressive strengths of simulated rocks at failure (MPa) at different lateral stresses (under triaxial compression test)

Rock Confining stress, KPa	Fayum argillaceous sand	Sinai coal	Red-Sea phosphate	Assiut limestone	Aswan granite
100	25.73	6.55	35.32	64.13	–
150	25.74	–	–	–	–
200	25.74	6.65	35.33	–	–
250	–	–	–	64.57	–
300	–	6.91	35.35	–	–
500	–	7.13	–	65.29	132.93
750	–	7.69	–	–	–
1000	–	–	–	–	145.83
2000	–	–	–	–	165.20
4000	–	–	–	–	203.95
6000	–	–	–	–	236.30

The effect of different lateral pressures on deviatoric stress was investigated through triaxial compression tests. The numerical analysis indicated that once a rock exceeds its elastic limit, shear stress is generated, and plastic flow may occur. In the case of Fayum argillaceous sand, the magnitude of deviatoric stress did not vary significantly with changing confining stresses. At 32 percent axial strain, the maximum difference between axial and lateral stress was recorded as 14.87 MPa. However, in Sinai coal, Red-Sea phosphate, Assiut limestone, and Aswan granite, deviatoric stress increased as confining stress increased. For instance, the highest deviatoric stresses for coal were observed at 5 MPa (at 45 percent axial strain), 25 MPa (at 50 percent axial strain), 42 MPa (at 38 percent axial strain), and 165 MPa (at 35 percent axial strain), respectively. Changes in confining stresses had negligible effects on the stress ratio in Fayum argilla-

ceous sand. Conversely, in Sinai coal, Red-Sea phosphate, Assiut limestone, and Aswan granite, the stress ratio increased with lateral stress and decreased with axial strain.

5. Conclusions

A series of experimental tests were conducted to investigate the strength characteristics of various types of rocks, including Fayum argillaceous sand, Sinai coal, Red-Sea phosphate, Assiut limestone, and Aswan granite. Numerical simulations using uniaxial and triaxial compression tests were employed to examine the stress-strain behavior during the failure process under different loading conditions. The conclusions drawn from the results can be summarized as follows:

1. The study primarily focuses on analyzing the influence of incremental displacement and confining stress on the peak strength of rocks during failure. By conducting numerical simulations, the researchers explored the relationship between these variables. The results indicate that an increase in confining stress leads to a higher peak strength of rocks at failure, which aligns with previous research [29], [30]. Furthermore, the study reveals that the effect of incremental displacement on the ultimate strength of rock diminishes as the displacement increases. However, the study does not address the impact of specimen size, leaving it as a potential area for future research.

2. In addition to investigating the peak strength, the study explores the behavior of volumetric strain, deviatoric stress, and stress ratio in relation to axial strain under different confining stresses. These aspects were thoroughly analyzed and interpreted within the context of numerical simulations. The findings shed light on the behavior of rocks under various loading conditions and provide valuable insights into their mechanical properties.

3. The study also examined the volumetric strain, which represents the change in the volume of the rock during triaxial compression. As the confining stress increased, both the volumetric strain and axial strain showed an upward trend.

4. Overall, this study demonstrates the reliability and effectiveness of numerical simulations as an alternative to traditional laboratory testing in rock mechanics. It showcases the ability of numerical modeling to accurately represent rock failure mechanisms and provides valuable information on the influence of incremental displacement and confining stress on rock strength.

6. Recommendations for future research

To validate the results obtained from numerical analysis, it is necessary to conduct experimental tests on rock samples under different incremental displacements and confining stresses to examine their macroscopic failure forms. Future research should also consider the influence of rock composition and mineralogy on failure mechanisms. Additionally, the application of Weibull distribution could be beneficial in explaining mineral composition and rock heterogeneity.

References

[1] Wawersik, W.R., & Fairhurst, C.H. (1970). A study of brittle rock fracture in laboratory compression experiments. *International Journal of Rock Mechanics and Mining Sciences & Geomechanics Abstracts*, 7(5), 561-575. https://doi.org/10.1016/0148-9062(70)90007-0

[2] Hudson, J.A. (1993). Rock properties, testing methods and site characterization. *Rock Testing and Site Characterization*, 1-39. https://doi.org/10.1016/B978-0-08-042066-0.50008-2

[3] Pells, P.J. (1993). Uniaxial strength testing. *Rock Testing and Site Characterization*, 67-85. https://doi.org/10.1016/B978-0-08-042066-0.50010-0

[4] Stoxreiter, T., Gehwolf, P., & Galler, R. (2020). Alternative approaches for the determination of unconfined rock deformation and strength properties. *Rock Mechanics and Rock Engineering*, (53), 411-433. https://doi.org/10.1007/s00603-019-01908-3

[5] Mardalizad, A., Scazzosi, R., Manes, A., & Giglio, M. (2018). Testing and numerical simulation of a medium strength rock material under unconfined compression loading. *Journal of Rock Mechanics and Geotechnical Engineering*, 10(2), 197-211. https://doi.org/10.1016/j.jrmge.2017.11.009

[6] Zhao, K., Gu, S., Yan, Y., Li, Q., Xiao, W., & Liu, G. (2018). Rock mechanics characteristics test and optimization of high-efficiency mining in Dajishan tungsten mine. *Geofluids*, (2018), 8036540. https://doi.org/10.1155/2018/8036540

[7] Wang, Z.H., Tan, Y.L., Li, S.M., Wang, T.Z., & Wu, X.C. (2021). Experimental and numerical study on mechanical properties and deformation behavior of Beishan granite considering heterogeneity. *Advances in Civil Engineering*, (2021), 6622958. https://doi.org/10.1155/2021/6622958

[8] Hammed, M.S.H. (2021). Strata-bound colonnade fractures in argillaceous sediments of Qasr El Sagha Delta, Fayum-Egypt. *Egyptian Journal of Geology*, 65(1), 55-72. https://doi.org/10.21608/EGJG.2021.103322.1010

[9] Kong, H., & Wang, L. (2014). Numerical calculation on the strength and failure rules of gassy coal during its failure process. *Electronic Journal of Geotechnical Engineering*, (19), 4655-4665.

[10] Hao, Z., & E-chuan, Y. (2015). The analysis of the schist's failure modes and mechanical characteristic in Northwest Hubei Province based on uniaxial and triaxial compression test. *Electronic Journal of Geotechnical Engineering*, (20), 6737-6760.

[11] Alshkane, Y. M. A. (2015). *Numerical modelling investigation of rock mass behaviour under gravity dams*. Doctoral Dissertation. Nottingham, United Kingdom: University of Nottingham. https://doi.org/10.13140/RG.2.1.2964.8486

[12] Lei, Y., Cheng, Y., Ren, T., Tu, Q., Shu, L., & Li, Y. (2021). The energy principle of coal and gas outbursts: experimentally evaluating the role of gas desorption. *Rock Mechanics and Rock Engineering*, (54), 11-30. https://doi.org/10.1007/s00603-020-02246-5

[13] Lockner, D.A. (1995). *Rock failure. Advancing Earth and space science*. Washington, United States: AGU.

[14] Hoek, E. (2001). *Rock mass properties for underground mines. Underground mining methods: Engineering fundamentals and international case studies*. Litleton, Colorado, United States: Society for Mining, Metallurgy and Exploration, 21 p.

[15] Vermeer, P.A., & De Borst, R. (1984). Non-associated plasticity for soils, concrete and rock. *HERON*, 29(3).

[16] Tan, X., Konietzky, H., & Frühwirt, T. (2015). Numerical simulation of triaxial compression test for brittle rock sample using a modified constitutive law considering degradation and dilation behavior. *Journal of Central South University*, 22(8), 3097-3107. https://doi.org/10.1007/s11771-015-2846-6

[17] Germanovich, L.N., Salganik, R.L., Dyskin, A.V., & Lee, K.K. (1994). Mechanisms of brittle fracture of rock with pre-existing cracks in compression. *Pure and Applied Geophysics*, (143), 117-149. https://doi.org/10.1007/BF00874326

[18] Griffith, A. (1924). *The theory of rupture. Proceedings of the first International Congress for Applied Mechanics*, 55-63.

[19] Healy, D., Jones, R.R., & Holdsworth, R.E. (2006). Three-dimensional brittle shear fracturing by tensile crack interaction. *Nature*, 439(7072), 64-67. https://doi.org/10.1038/nature04346

[20] Hoek, E., & Brown, E.T. (2019). The Hoek-Brown failure criterion and GSI-2018 edition. *Journal of Rock Mechanics and Geotechnical Engineering*, 11(3), 445-463. https://doi.org/10.1016/j.jrmge.2018.08.001

[21] *RS2D, Rock and Soil 2-dimensional analysis program*. (2016). Toronto, Ontario, Canada. Retrieved from: https://www.rocscience.com/software/rs2

[22] Brown, E.T. (2008). Estimating the mechanical properties of rock masses. *Proceedings of the First Southern Hemisphere International Rock Mechanics Symposium*, 3-22.

[23] Eberhardt, E. (2012). The Hoek-Brown failure criterion. *Rock Mechanics and Rock Engineering*, (45), 981-988. https://doi.org/10.1007/s00603-012-0276-4

[24] Wang, S.Y., Sloan, S.W., Sheng, D.C., Yang, S.Q., & Tang, C.A. (2014). Numerical study of failure behaviour of pre-cracked rock specimens under conventional triaxial compression. *International Journal of Solids and Structures*, 51(5), 1132-1148. https://doi.org/10.1016/j.ijsolstr.2013.12.012

[25] Stefanizzi, S., Barla, G., Kaiser, P., & Grasselli, G. (2009). Numerical modeling of standard rock mechanics laboratory tests using a finite/discrete element approach. *Proceedings of the 3rd CANUS Rock Mechanics Symposium, Toronto*.

[26] Mahabadi, O.K., Lisjak, A., Grasselli, G., Lukas, T., & Munjiza, A. (2010). Numerical modelling of a triaxial test of homogeneous rocks using the combined finite-discrete element method. *ISRM International Symposium-EUROCK*.

[27] Paterson, M.S., & Wong, T.F. (2005). *Experimental rock deformation: The brittle field*. Berlin, Germany: Springer, 358 p.

[28] Smoljanović, H., Živaljić, N., & Nikolić, Ž. (2013). A combined finite-discrete element analysis of dry-stone masonry structures. *Engineering Structures*, (52), 89-100. https://doi.org/10.1016/j.engstruct.2013.02.010

[29] Tiankui, G., & Zeming, D. (2021, March). Meso-numerical simulation of rock triaxial compression based on the damage model. *IOP Conference Series: Earth and Environmental Science*, 687(1), 012134. https://doi.org 10.1088/1755-1315/687/1/012134

[30] Komurlu, E. (2018). Loading rate conditions and specimen size effect on strength and deformability of rock materials under uniaxial compression. *International Journal of Geo-Engineering*, (9), 1-11. https://doi.org/10.1186/s40703-018-0085-z

Чисельне моделювання механічної поведінки зразків гірських порід під час випробувань на одновісне та тривісне стискання

В.Р. Абделлах, С.А. Бадер, Ю.-Г. Кім, М.А.М. Алі

Мета. Вивчення впливу навантаження на межу міцності гірських порід на одновісне та тривісне стискання, із застосуванням різних утримуючих напружень, збереженням постійного осьового напруження на стискання та поступового збільшення зміщення.

Методика. Для проведення дослідження дослідники використовують програмне забезпечення для аналізу породи і ґрунту RS2D для вивчення впливу різних додаткових зміщень і утримуючих напружень на міцнісні властивості різних зразків гірських порід. Чисельний аналіз включає дослідження наступних порід: фаюмський глинистий пісок, синайське вугілля, асуанський граніт, асьютський вапняк і фосфат Червоного моря.

Результати. Результати дослідження свідчать про те, що межа міцності гірських порід на стискання при руйнуванні досягається при незначних додаткових зміщеннях. Встановлено, що збільшення утримуючого напруження призводить до більш високої межі міцності на розтяг, девіаторних напружень та об'ємної деформації, однак фактор напруження зменшується залежно від відсотка осьової деформації.

Наукова новизна. Чисельним моделюванням на основі критерію руйнування Мора-Кулона надано аналіз наступних результатів: кривих напруження-деформації (σ-ε), відношення напружень (σ_1 / σ_3), девіаторних напружень ($\sigma_1 - \sigma_3$) та об'ємної деформації залежно від відсотка осьової деформації.

Практична значимість. Використовуючи аналіз чисельного моделювання, стає можливим відтворити механізми руйнування гірських порід, що спостерігаються під час випробувань на одновісне та тривісне стискання. Ця методологія має потенціал для зменшення потреби у великих експериментальних випробуваннях в оцінці межі міцності гірських порід на розтяг при різних навантаженнях. У результаті час та витрати можуть бути зведені до мінімуму.

Ключові слова: *випробування на одно- і тривісне стискання, чисельне моделювання, швидкість зміщення/деформації, утримуючі напруження, криві напруження-деформаці, девіаторні напруження*